applied sciences

MDPI

Article

Development of Alfa Fiber-Based Mortar with Improved Thermo-Mechanical Properties

Siham Sakami [1], Lahcen Boukhattem [2,3,*], Mustapha Boumhaout [2] and Brahim Benhamou [2,4]

1 L3G, Faculty of Sciences and Techniques, Cadi Ayyad University, Marrakesh 40000, Morocco; s.sakami@uca.ma
2 EnR2E Laboratory, National Center of Studies and Research on Water and Energy, CNEREE, Cadi Ayyad University, Marrakech 40000, Morocco; mustapha.boumhaout@edu.uca.ac.ma (M.B.); BBenhamou@uca.ma (B.B.)
3 LMPEQ, National School of Applied Sciences, Cadi Ayyad University, Safi, Marrakech 46000, Morocco
4 ProcEDE Laboratory, Cadi Ayyad University, Marrakech 40000, Morocco
* Correspondence: l.boukhattem@uca.ma

Received: 10 October 2020; Accepted: 6 November 2020; Published: 12 November 2020



Abstract: This work deals with the development of a new composite based on mortar reinforced with optimally sized alfa fiber (AF). Experimental investigations of physical and thermo-mechanical properties of the new AF mortar composite are performed for AF weight fraction varying from 0% to 5%. This simple material preparation process is described and scanning electron microscopy (SEM) is undertaken to analyze the morphology of this composite. It shows a random dispersion of the AF into the mortar matrix. Physical properties such as open porosity, water absorption, and bulk density fluctuations with AF mass content are measured. Measured thermal conductivity is compared to the values generated by different prediction models. Good agreement, within 9.6%, is obtained with data predicted by Woodside–Messmer's method. It is demonstrated that this simple blending of AF into mortar improves significantly the thermo-mechanical behavior of the new composite. An addition of 5% of AF weight content makes composite material lighter by about 15%, enhances its insulating thermal capabilities by about 57% and increases its heat diffusion damping rate by about 49%. Moreover, the composite mechanical (flexural and compressive) strength increases by up to 10% for an AF weight content of 1%.

Keywords: alfa fiber; cement; composite; density; mechanical properties; thermal properties

1. Introduction

Recently, the use of natural plant fibers as reinforcement to concrete has become very attractive [1]. This is due to the increase of environmental awareness and to the advantages of these fibers such as availability, recyclability, low cost, environmentally friendly, harmlessness, abrasion free, biodegradability, and better thermo-mechanical performance when compared to conventional fibers. Different natural fibers (date palm, cotton, sisal, flax, hemp, jute, ramie, kenaf, bamboo, banana, coir, coconut and wheat straws) could be good candidates for blending with other compounds (cement, clay, sand, lime, gypsum, mortar, concrete, etc.) in order to develop new thermal insulating composite materials. Therefore, several studies have been conducted on various vegetable fibers from sisal [2], coconut [3], hemp [4], kenaf [5], banana [6], date palm [7], bamboo [8], jute [9] to alfa fiber [10].

The alfa plant, also called esparto grass stems (*Stipa tenacissima*), grows abundantly in the Mediterranean basin, especially in countries such as Spain, Italy, Libya, Tunisia, Algeria, and Morocco. This fiber is a permanent plant that does not disappear during winter and grows in independent

shrubs where it can reach a height between 1 to 1.20 m [11]. It covers many million hectares in this area, with about 4,000,000 ha in Algeria, 3,186,000 ha in Morocco, 600,000 ha in Tunisia, 350,000 ha in Libya, and 300,000 ha in Spain [12]. The annual production is approximately 250,000 t in Algeria, 125,000 t in Morocco, and 75,000 t in Tunisia [13].

Alfa fiber is selected in this study thanks to its high availability in dry region and its interesting thermo-mechanical properties. Its thermal conductivity can be as low as 0.042 $W{\cdot}m^{-1}{\cdot}K^{-1}$ [14] which is in the same order of magnitude as hemp and flax [15]. Moreover, it has a better mechanical strengths as reported in the previous studies [16,17]. These properties make alfa fiber (AF) a reinforcement candidate for mineral materials. In building construction field, several researchers have dealt with the manufacturing of AF cementitious composite materials.

Krobba et al. [18] performed an experimental study on a repair mortar based on dune sand and microfibers with various volume percentages, lengths (3 to 5 mm) and diameters (150–200 μm). The results showed that the use of 0.75% of alfa micro-fiber increases mechanical properties of mortar.

Jabali et al. [19] studied the influence of different volume fractions of long alfa fibers (150 mm) on thermomechanical performance of mortar-based composite. This procedure is very labor extensive since the AF is distributed as a single layer within the mortar slab at a specific depth. They measured a reduction in thermal conductivity of 37% at 1.5% of alfa fiber content and an improvement of flexural strength by up to 27% for 1% of AF.

Elhamdouni et al. [20] presented a comparative study of thermo-mechanical properties of two materials: clay/alfa and clay/straw. They showed that for a weight fraction of fiber above 2% the adhesion between fiber and clay becomes very low which in turn affects the mechanical performance of these two composite materials.

On the other hand, interest in these new composite materials has drawn researcher's attention to developing new prediction tools to estimate the new composite thermal conductivity. Braiek et al. [21] have compared experimental results and theoretical equivalent thermal conductivity of materials with two phases, continuous gypsum phase and dispersed date palm fibers phase. Taoukil et al. [22] have carried out a comparison of experimental and theoretical approaches of the material's thermal conductivity with two-phase medium made up of mortar matrix and wood wool insulator.

Despite the extensive research work on alfa fiber in construction materials, this fiber is still not heavily used in building. The objective of this work is to present a procedure to build the AF mortar composite and to investigate the improvement of its thermo-mechanical properties in order to bring more attention to the potential of this abundant renewable resource of AF (which is mostly used in handcrafts only) in material building in the Mediterranean region.

A complete analysis of the effect of mortar blending with AF on physical and thermomechanical properties was executed for different weight fraction (ω) from 0% to 5%.

In the first part of this paper, the material preparation process is described; the elaborated new composites were scanned by the SEM to determine their morphology. In the second part, experimental measurements of the thermomechanical properties such as thermal conductivity, thermal diffusivity, flexural and compressive strengths were carried out. Moreover, mathematical models were used to compare predicted and measured thermal conductivities of the composite materials at dry state. These theoretical models have been developed/used by different researchers to calculate the equivalent thermal conductivity value of composite materials at dry state; they combine in different ways the thermal conductivity of two phases: solid phase (solid matrixes of mortar and fibers) and air phase in composites. These models were rearranged in this work to be applied for three phases: solid matrix of mortar, solid matrix of alfa fiber and air. The purpose of this comparison, between predicted and measured thermal conductivities as a function of volume percentage of AF's solid matrix (φ), is to demonstrate that the model that captures well the distribution of the three phases within the composite material is in good agreement with the experimental data.

2. Materials and Methods

2.1. Material Selection

The new composite material manufacturing consists of mixing cement, sand and alfa fiber (AF) with drinking tap water. The AF plant used to reinforce mortar was extracted from the Oujda region in the northeast of Morocco (Figure 1a). It was prepared in different steps. It was first prepared by submerging it in a salt water (35 $g{\cdot}L^{-1}$) [23] at ambient temperature (about 30 °C) for 7 days and was washed with water jet. The goal of this soaking process was to remove sand and dust existing on the stem surface and to facilitate fiber separation. Subsequently, the plant stems were dried under the sun for one week. These low cost and environmental operations will eliminate most of the moisture in alfa stems and consequently make the grinding operation more efficient. The dried alfa stems were crushed (Figure 1b), separated, and cut into short fibers with a diameter between 0.7 and 1 mm, and a length between 1.5 and 2.5 cm (Figure 1c). These lengths were selected since [24] demonstrated that optimal mechanical performance was obtained at this length range.

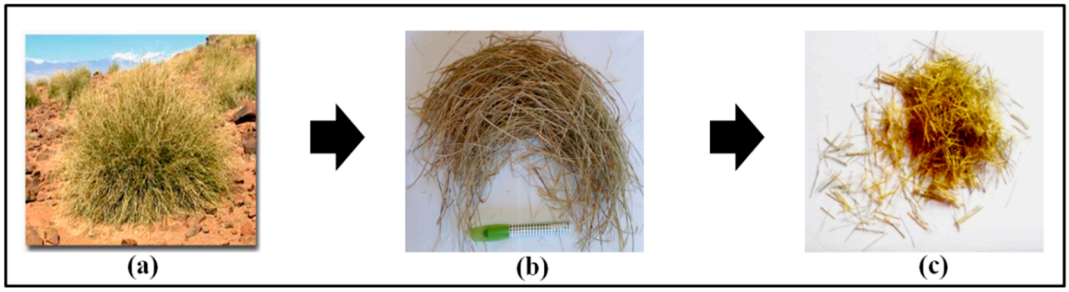


Figure 1. Steps of alfa fiber (AF) preparation: (**a**) alfa plant, (**b**) crushed alfa stem after drying process and (**c**) used AF.

This natural treatment of AF will enhance the fibers adhesion with the cementitious matrix.

An alfa fiber diffractogram obtained from an X-ray diffractometry (XRD) test is shown in Figure 2. One can clearly notice that the spectrum contains two main peaks. The first one, wide and multiple, is obtained at Bragg angles of 15° and 16.54° corresponding to crystallographic planes of (1–10) and (110), respectively. The second one appears at 22.50° which is associated to a crystallographic plane of (200). These two peaks are characteristic of the presence of cellulose I. The cellulose component is considered as a bio-binder that can bond efficiently the fibers to mortar.

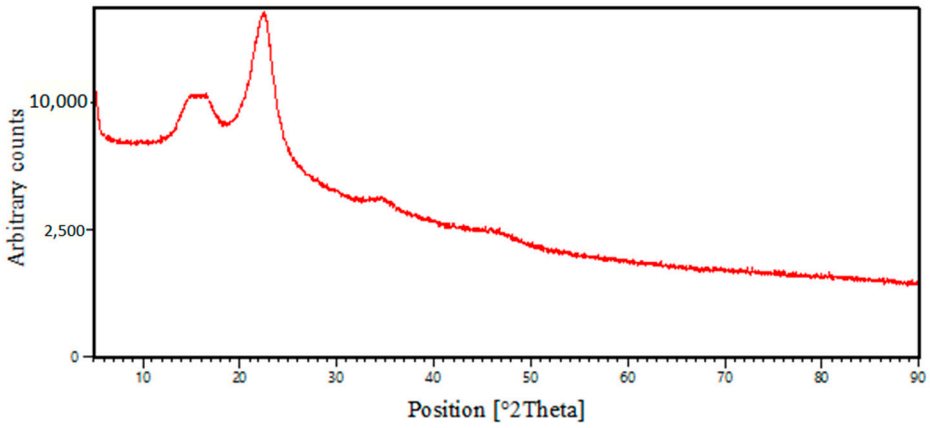


Figure 2. Alfa fiber X-ray diffractogram.

The Portland (CPJ 35- CEM II 22.5) cement is used in this study, and its technical characteristics are in agreement with the Moroccan norm (NM 10.01.004., 2003) [25]. The sand used is extracted from

Nafiss River (Loudaya, Morocco) with a maximum size of 2 mm and water mass content of 2.15%. The sand equivalent test indicates that the average value of its neatness is 87% (NF EN 933-8, 1999) [26]. Its chemical constitution is reported in Table 1.

Table 1. Chemical constitution of used sand.

Constituents	SiO_2	Al_2O_3	K_2O	Fe_2O_3	Na_2O	MgO	CaO	P_2O_5	TiO_2	SO_3	Cl
Content (%)	68.51	13.55	3.95	2.83	2.72	2.64	1.62	0.16	0.7	0.01	0.005

2.2. Preparation of the Alfa Fiber Composite Test Specimens

The preparation of the test samples consists of substitution of sand with different AF mass fractions to evaluate the impact on the thermo-mechanical properties compared to those of the reference mortar (RM). The latter was made from sand-cement with a mass ratio of 3 and a water-cement mass ratio of 0.6. Afterward, in addition to RM, five other new composite materials, labeled AFRM0.5%, AFRM1%, AFRM2%, AFRM3.5% and AFRM5%, were obtained by incorporating respectively the AF mass percentages of 0.5%, 1%, 2%, 3.5% and 5% into mortar. Prismatic molds of dimensions $4 \times 4 \times 16$ cm^3 were used for mechanical tests while parallelepiped molds with dimension of $26.4 \times 26.4 \times 4$ cm^3 were used for thermo-physical measurements (Figure 3a–c). All molds were filled with the mixed components and cured in the laboratory for 24 h under normal weather conditions: $T = 20 \pm 2$ °C and relative humidity $RH = 65 \pm 5\%$. After demolding operation, the samples were placed in water at ambient temperature for 28 days, according to the norm (NF EN 196-1, 1995) [27]. Finally, for each AF mass percentage, three manufactured samples of AFRM composites were tested to determine the average values and uncertainties of thermo-mechanical properties. The manufactured samples are shown in Figure 3d–f.

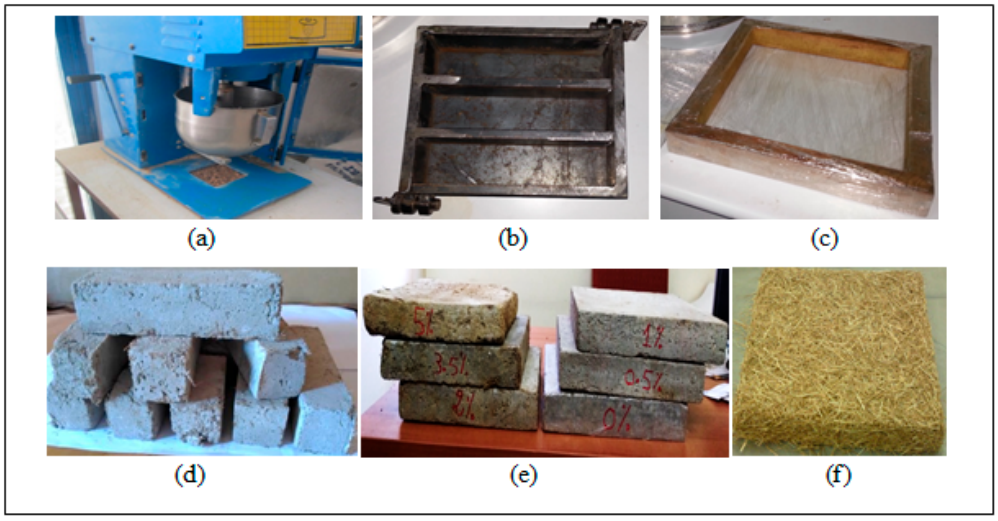


Figure 3. Preparation and manufactured samples: (**a**) mixer, (**b**,**c**) prismatic and parallelepiped molds, (**d**,**e**) samples for mechanical and thermal tests and (**f**) AF binderless board.

2.3. Measurement Instruments and Experimental Methods Description

2.3.1. Scanning Electron Microscopy (SEM) Morphological Observation

A TESCAN ORSAY (VEGA3) scanning electron microscope (SEM) was used to observe the morphology of AFRM composite and examine the homogeneity and distribution levels of AF in mortar matrix. It is a versatile tungsten thermionic emission system intended for both high and low void processes. VEGA3 is fitted with an electron optics system based on a unique four-lens wide field optics design with a proprietary intermediate lens. The SEM pictures were taken with beam acceleration at 5 kV.

2.3.2. Open Porosity, Water Absorption, and Bulk Density

Open porosity P_0, water absorption W_a, and bulk density ρ_b measurements were conducted to determine the quality of mortar-AF composite materials. Their values were obtained by the Archimedes method of triple weighing, in agreement with the Standards Methods Designation: American society for testing and materials (ASTM C20–00) [28]. Immersion liquid used for these tests was clean water. Knowing dry weight (m_{dry}), soaked weight (m_{sat}) and hydrostatic weight (m_{hyd}) of the studied AFRM composites, the corresponding open porosity, water absorption, and bulk density are calculated respectively by Equations (1)–(3):

$$P_0 = \frac{m_{sat} - m_{dry}}{m_{sat} - m_{hyd}} \times 100 \quad (1)$$

$$W_a = \frac{m_{sat} - m_{dry}}{m_{dry}} \times 100 \quad (2)$$

$$\rho_b = \frac{m_{dry}}{m_{sat} - m_{hyd}} \times \rho_{water} \quad (3)$$

2.3.3. Thermo-Mechanical Characterization Methods

The EI700 device (two boxes method) was used to determine the thermal properties of insulating building materials [29]. It contains two boxes designed to take measurements in similar conditions. The first box was reserved for thermal conductivity k measurement and the second box was dedicated to thermal diffusivity α measurement Figure 4c. The process used to measure these two parameters was detailed in a previous study by Boumhaout et al. [30].



Figure 4. Devices used for thermo-mechanical tests: (**a**) air conditioned chamber, (**b**) two boxes method, (**c**) boxes of measured thermal conductivity and diffusivity, (**d**) flexural test, (**e**) two half prisms obtained from flexural test and (**f**) compressive test.

The accuracy of thermal conductivity measurement at steady state can be affected by ambient conditions variation. An air-conditioned chamber (see Figure 4a,b) was built to maintain the instrument surroundings at constant temperature during the experiment. Therefore, the experiment can be completed in a reduced duration between 6 and 10 h.

The device 270 kN capacity I20 201 press with velocity loading fixed at 500 ± 10 $N{\cdot}s^{-1}$ and 2400 ± 200 $N{\cdot}s^{-1}$ was used for mechanical testing. The measurements of flexural and compressive strengths were performed after 28 days of specimens curing process, according to the Moroccan norm (NM 10.1.005., 1994) [31] (Figure 4d,f). The flexural strength measurement method of prismatic specimen was determined by a three points bending technique. The two half prisms (Figure 4e) obtained from this test were used for compressive strength measurement (Figure 4f).

2.4. Thermal Conductivity Prediction Models

Many researchers have developed theoretical models to calculate the equivalent thermal conductivity value of composite materials. These models combine in different ways the thermal conductivity of two phases in composite materials at dry state: solid phase (solid matrixes of mortar and fibers) and air phase. These models were rearranged in this study to be applied for three phases: solid matrix of mortar, solid matrix of alfa fiber and air. Table 2 provides the rearrangement expressions of seven models presented in the literature (fourth column of Table 2). These models were applied to calculate the thermal conductivity of AFRM composites for different volume ratios of AF's solid matrix φ.

Table 2. Theoretical models.

Model	Equation		Comment	Reference
Parallel	$k_{//} = \varphi(1-P_t)k_{i-f} + (1-P_t)(1-\varphi)k_{i-M} + P_t k_a$	(4)	φ: Volume ratio of solid matrix of AF per absolute volume of sample. $\rho_{abs\ RMAF}$: Absolute density of composite. P_t: Total porosity. k_{i-f} and k_{i-M}: Intrinsic thermal conductivities of AF and reference mortar (RM) respectively. k_a: Thermal conductivity of air. ω: Weight content of AF per weight of mixture. ρ_b: Bulk density of composite. $\rho_{abs\ RM}$ and $\rho_{abs\ AF}$: Absolute densities of reference mortar and AF.	[32–34]
	$\varphi = \frac{\rho_{abs\ RMAF} - \rho_{abs\ RM}}{\rho_{abs\ AF} - \rho_{abs\ RM}}$	(5)		
	$\rho_{abs\ RMAF} = \frac{1}{\omega \times \left(\frac{1}{\rho_{abs\ AF}} - \frac{1}{\rho_{abs\ RM}}\right) + \frac{1}{\rho_{abs\ RM}}}$	(6)		
	$P_t = \left(1 - \frac{\rho_b}{\rho_{abs\ RMAF}}\right) \times 100$	(7)		
Serial	$k_{\perp} = \frac{1}{(\varphi/k_{i-f}) + (1-(\varphi+P_t))/k_{i-M} + P_t/k_a}$	(8)		
Beck's	$k = \sqrt{k_{\perp} k_{//}}$	(9)		
Woodside and Messmer	$k = k_{i-f}^{\varphi(1-P_t)} k_{i-M}^{(1-P_t)(1-\varphi)} k_a^{P_t}$	(10)		
Auto-coherent	$k = k_{i-M}\left[1 + \frac{\tau}{(1-\tau)/3 + \frac{3+\delta\left(k_a/k_{i-M}-1\right)}{3\left(k_a/k_{i-M}-1\right) - \delta\left(k_a/k_{i-f}-1\right)\left(2k_{i-f}/k_{i-M}+1\right)}}\right]$	(11)	$\tau = (1-\varphi)P_t + \varphi$: Volume ratio of (air + AF) in the sample. $\delta = 1 - \frac{P_t}{\tau}$: Concentration of AF in relation to components (air + AF) in the sample.	[35–37]
Effective medium theory (EMT)	$\sum_j \phi_j\left(\frac{k-k_j}{k+k_j}\right) = 0$	(12)	$\phi_f = \varphi(1-P_t)$: Volume ratio of solid matrix of AF per volume of sample. $\phi_M = (1-P_t)(1-\varphi)$: Volume ratio of solid matrix of mortar per volume of sample. $\phi_a = P_t$: Volume ratio of solid matrix of air per volume of sample.	[38,39]
	$\phi_f\left(\frac{k-k_{i-f}}{k+k_{i-f}}\right) + \phi_M\left(\frac{k-k_{i-M}}{k+k_{i-M}}\right) + \phi_a\left(\frac{k-k_a}{k+k_a}\right) = 0$	(13)		
Krischer–Kroll	$k = \frac{1}{(1-\varepsilon)/k_{//} + \varepsilon/k_{\perp}}$	(14)	ε: Volume fraction of the layers oriented perpendicular to the heat flux direction	[40]

The goal is to determine the effect of the three components (mortar, air and AF) distribution on the predicted thermal conductivity and to compare them to the measurement data.

3. Results and Discussions

3.1. SEM Morphological Analysis of the Alfa Fiber Reference Mortar (AFRM) Composites

Scanning electron microscopy was used to analyze the morphology of AFRM composites. The analysis of the SEM pictures displayed in Figure 5 indicates clearly that alfa fibers are randomly dispersed, separated, and embedded into mortar matrix. Moreover, all pictures show that the fiber surfaces are impregnated with mortar paste, which could indicate good bonds between AF and the surrounding solid matrix. The voids observed in Figure 5e,f between alfa fibers and mortar matrix could be generated due to the drying operation, worse miscibility, and lower fiber dispersion in the mortar.

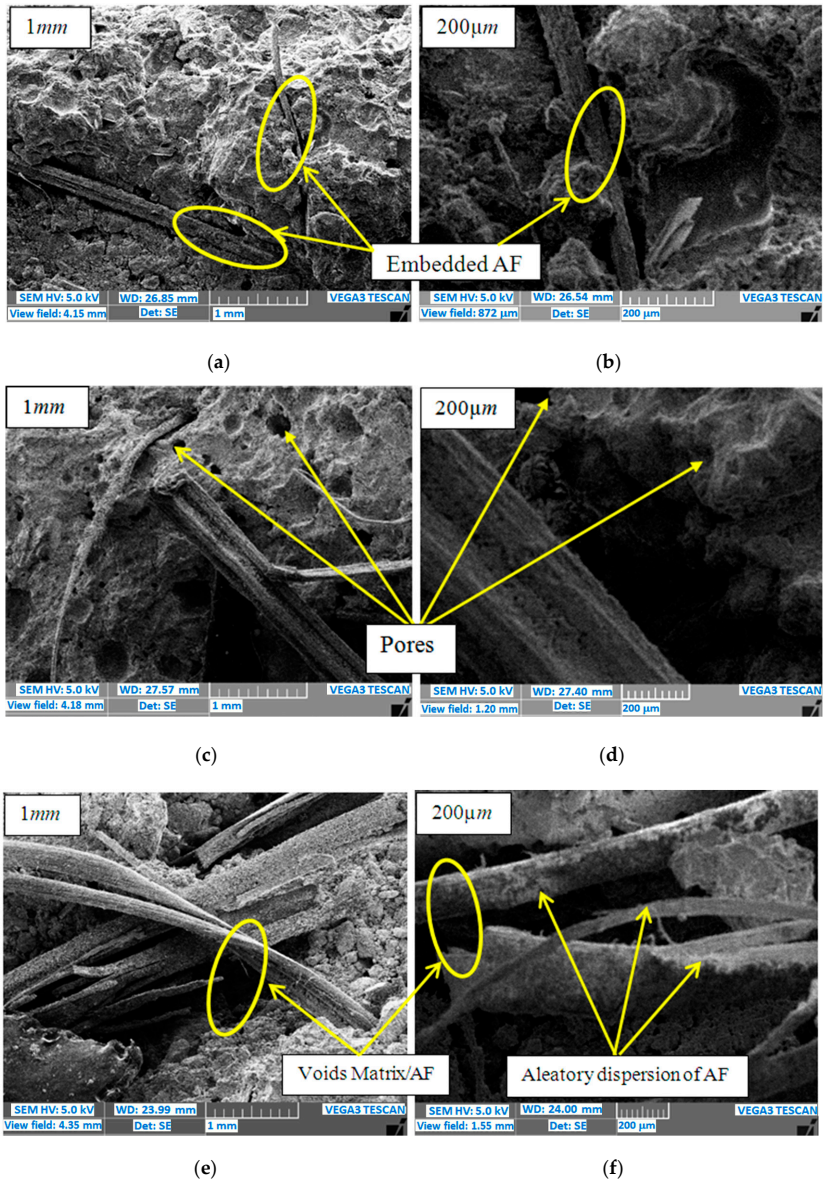


Figure 5. Scanning electron microscope (SEM) pictures of composites at two different scale lengths 1 mm and 200 µm: (**a**,**b**) AFRM 1%, (**c**,**d**) AFRM 2%, (**e**,**f**) AFRM 5%.

3.2. Thermophyical Performance Analysis

3.2.1. Open Porosity, Water Absorption, and Bulk Density

The fluctuations of open porosity, water absorption, and bulk density of composites as a function of AF are presented respectively in Figure 6a,b and Figure 7. It can be seen that the addition of AF leads to an increase in porosity by a factor up to 48.71%, an increase of water absorption by about 74% due to the hydrophilic character of AF, and a decrease of the density by about 14.68% for 5% of AF mass content. This is expected since the AF density (247 kg·m^{-3}) is lower than that of mortar (1748 kg·m^{-3}). These results can also be explained by the formation of voids at the inter-facial areas between AF and solid matrix due to the air bubbles trapping by fibers during the mixing and drying processes.

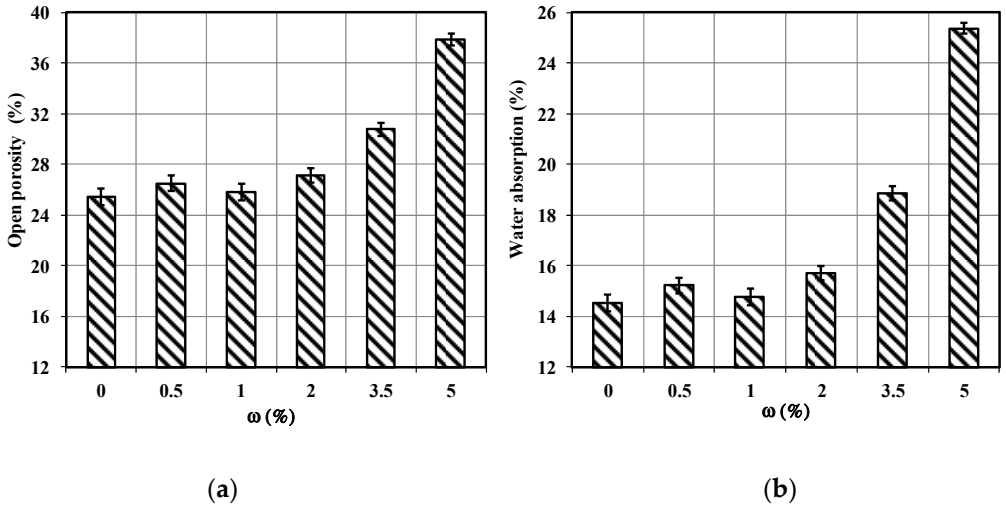


Figure 6. Effect of AF mass content at day 28 on open porosity (**a**) and on water absorption (**b**). Measurements uncertainties are respectively below 0.7% and 0.33%.

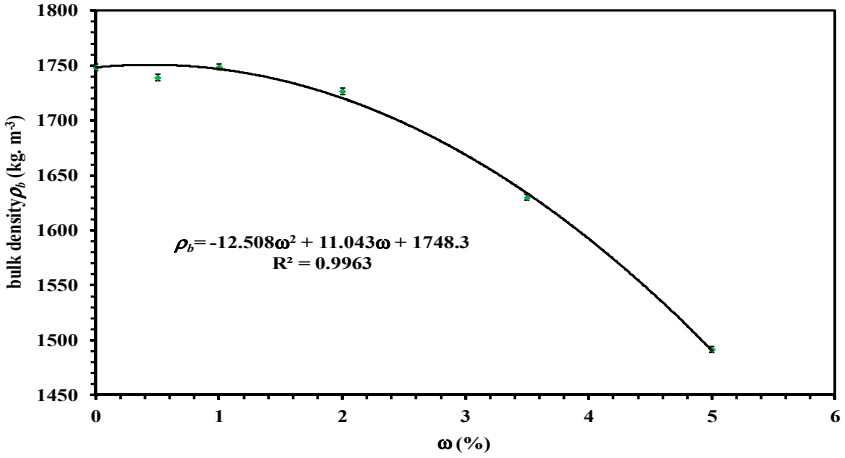


Figure 7. Effect of AF mass ratio on bulk density at day 28. Measurements uncertainty is below 0.2%.

Moreover, porosity and water absorption of AFRM1% slightly decrease respectively by 2.4% and 3% compared to AFRM0.5% while the bulk density remains nearly constant from 0% to 1% of AF inclusion. Furthermore, mortar reinforced with 1% of AF yields to good homogeneity and a better consolidated structure of the composite as indicated in the SEM pictures (Figure 5a).

In order to determine the thermal properties of composites at dry state, all prepared specimens were placed in a drying oven at 105 ± 1 °C with relative humidity of about 30% until mass stabilization within ±2 g for 24.

3.2.2. Thermal Conductivity Measurements

It can be observed from Figure 8 that the thermal conductivity of AFRM composite decreases with increasing fibers weight content, and consequently increases its thermal insulation capacity. The thermal conductivity of the reference mortar of about 0.809 $W{\cdot}m^{-1}{\cdot}K^{-1}$ drops to 0.347 $W{\cdot}m^{-1}{\cdot}K^{-1}$ for AFRM5%, corresponding to an improvement in insulation performance of around 57%. A similar result was reported by [19] who used a single layer fully made of AF with a length of 15 cm as reinforcement at a specific depth inside the cementitious matrix.

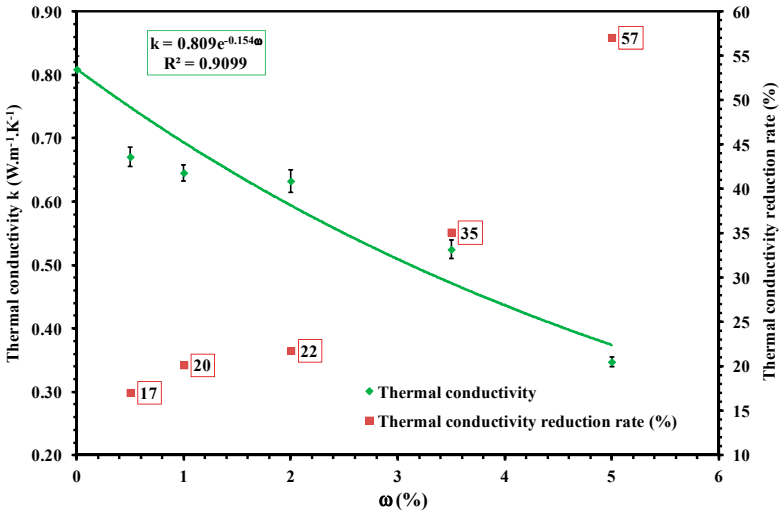


Figure 8. Thermal conductivity (primary axis) and its reduction rate (secondary axis) as function of AF mass content. Measurements uncertainty is below 2.9%.

This behavior is expected and can be explained by two arguments. First, the natural fibers are known to have lower thermal conductivities than those of mortar solid matrixes. The measured bulk thermal conductivity of AF binderless board and mortar are 0.056 ± 0.002 $W{\cdot}m^{-1}{\cdot}K^{-1}$ and 0.809 $W{\cdot}m^{-1}{\cdot}K^{-1}$ respectively. Second, the presence of fibers in solid matrix produces voids as shown in SEM pictures Figure 4e, causing growth in open porosity and a reduction in bulk density of AFRM composite. The latter becomes then more thermally insulating. This phenomenon is always taking place on composite with mineral matrix and vegetable fibers according to several works [41–43].

3.2.3. Intrinsic Thermal Conductivities Determination

The thermal conductivity prediction models shown in Table 2 require some parameters to be first determined. Solid matrix thermal conductivity k_{i-M} of RM is determined by solving a system of two unknowns (k_{i-M} and ε) ([40,44–46]):

$$\varepsilon_{dry}(k_{i-M}) = \frac{k_{\perp}\left(k_{//} - k_{dry}\right)}{k_{dry}(k_{//} - k_{\perp})} \quad (15)$$

$$\varepsilon_{sat}(k_{i-M}) = \frac{k_{\perp}(k_{//} - k_{sat})}{k_{sat}(k_{//} - k_{\perp})} \quad (16)$$

$\varepsilon_{dry}(k_{i-M})$ and $\varepsilon_{sat}(k_{i-M})$ are respectively the values of ε at dry and saturated states of the sample. k_{dry} and k_{sat} are the thermal conductivities of the RM measured respectively at dry and saturated states.

The measured thermal conductivity of saturated RM sample is $k_{sat} = (1.06 \pm 0.02)$ W·m^{-1}·K^{-1}. The determination of k_{i-M} and ε is undertaken by using Newton's method, which consists in determining by successive approaches, in Scilab Software, the value of k_{i-M} for which:

$$\varepsilon_{dry}(k_{i-M}) = \varepsilon_{sat}(k_{i-M}) \quad (17)$$

where $k_{i-M} = 2.58$ W·m^{-1}·K^{-1}

$k_{i-f} = 0.21$ W·m^{-1}·K^{-1} is determined according to Beck's model Equation (9) at dry state of AF binderless board (the measured value is $k_{BB} = (0.056 \pm 0.02)$ W·m^{-1}·K^{-1}).

Total porosities and absolute densities of composites, and absolute density of fiber are given in Table 3.

Table 3. Required parameters for thermal conductivity prediction.

Composites	RM	AFRM 0.5%	AFRM 1%	AFRM 2%	AFRM 3.5%	AFRM 5%
P_t (%)	28.10	28.20	27.46	27.72	30.84	35.86
$\rho_{abs\ RMAF}$(kg·m^{-3})	2433	2422	2411	2389	2357	2326
$\rho_{abs\ AF}$(kg·m^{-3})	1263					

3.2.4. Predicted Thermal Conductivities Comparison

Experimental and theoretical data of thermal conductivity are displayed in Figure 9 as function of AF intrinsic volumetric fraction per absolute volume of sample, φ.

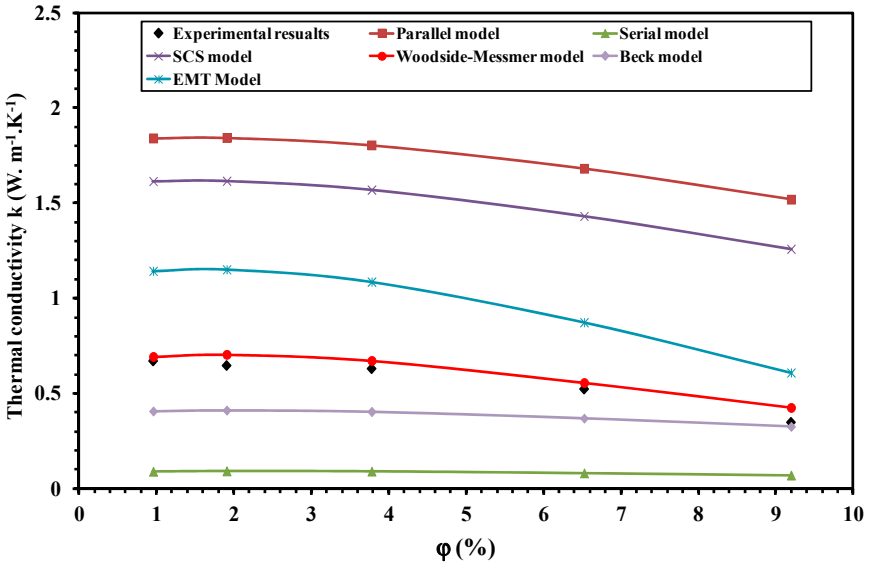


Figure 9. Comparison between measured and calculated thermal conductivities of AFRM composites as function of φ.

At first glance, one can remark that the measured thermal conductivities are between extreme values represented by parallel model (upper limit) and serial model (lower limit). They are respectively away from parallel model by about 221% and serial model by about 84.5%. The Auto-coherent model assumes all composite constituents to have a spherical shape, which is not the case for AF (see Figure 5). That explains the disagreement between the results obtained by this model and the experimental measurements which show a mean relative error of 175%. The results obtained by the effective medium theory (EMT) model are shifted from the experimental ones by about 73%. Beck's model prediction shows smaller difference with the experimental measurements with a mean relative error of 29%, because some alfa fibers have parallel and serial distributions.

The model that better predicts the measured thermal conductivities is Woodside and Messmer's model, with a mean relative error within 9.6%. This can be explained by the fact that the three phases (solid matrix, AF, and air) distribution as observed in SEM images of AFRM composites (Figure 5) is well captured by Woodside and Messmer's model. This finding can help in the future limit the need for additional thermal conductivity measurements if one has sufficient a priori information.

3.2.5. Thermal Diffusivity

The thermal diffusivity variation of AFRM composite as function of mass AF ratio is displayed in Figure 10. The thermal diffusivity is reduced by a factor of about 51% for 5% of AF mass content in the mixture. The heat transfer in the AFRM sample is damped due to the porosity growth within the sample with AF mass content increase, and to the alveolar arrangement of AF which resists the heat diffusion. It is observed from Figure 7 that the density, which was obtained from an independent measurement, decreases with AF content. Calculated specific heat (Figure 11) decreases as well for AF content below 1%. Thus, this decrease in thermal diffusivity is mainly driven by the thermal conductivity.

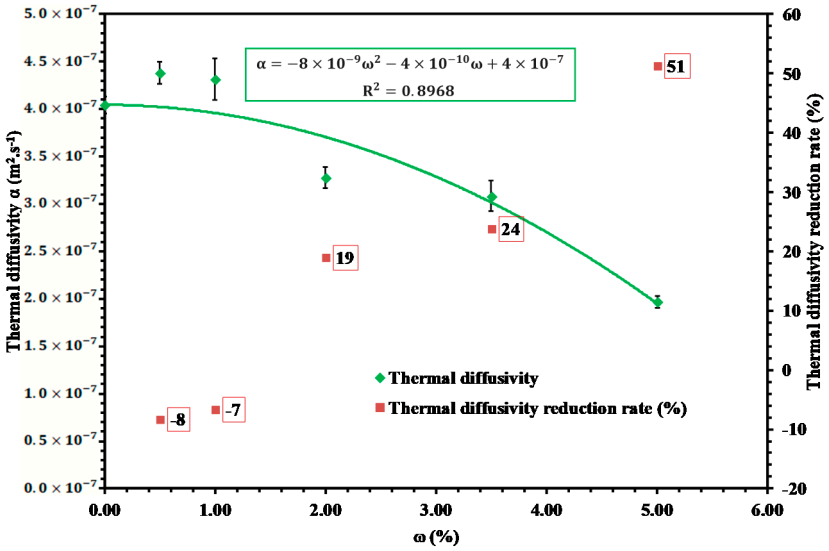


Figure 10. Thermal diffusivity (primary axis) and its reduction rate (secondary axis) as function of AF mass content. Measurements uncertainty is below 5.22%.

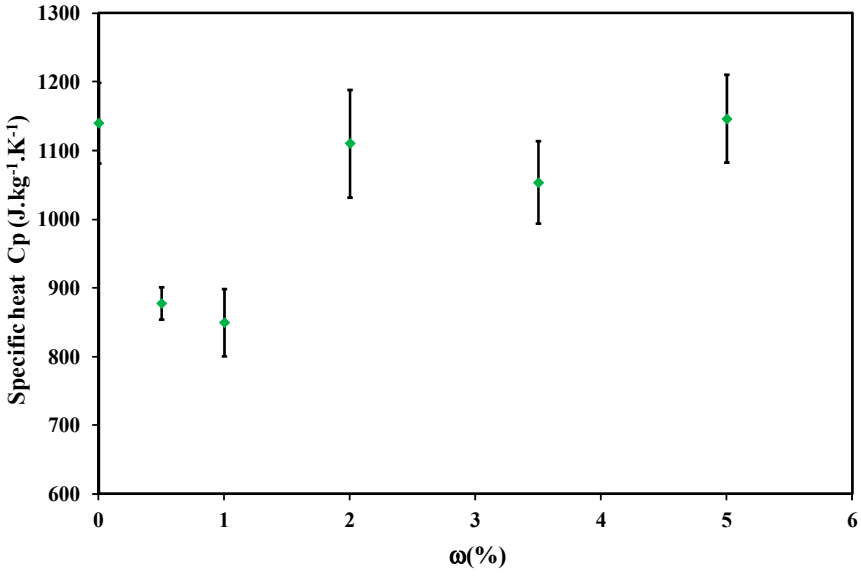


Figure 11. Specific heat variation with alfa fiber mass content. Measurements uncertainty is below 7%.

In addition, the thermal diffusivity of mortar, with no AF, ($4.04 \pm 0.0886\ 10^{-7}\ m^2 \cdot s^{-1}$) is greater by about four times than the measured one of AF ($0.98 \pm 0.04\ 10^{-7}\ m^2 \cdot s^{-1}$), which obviously impacts the thermal diffusivity of the composite material.

3.3. Time-Lag

Time-lag (TL) is defined as the time duration between two associated occurrences such as a cause and its effect. In our case, it is the time interval during which the heat flow peak passes through a flat slab from one side to another. The time-lag was calculated based on measured thermal diffusivity values using the following expression [47]:

$$TL = \frac{1}{2} e \sqrt{\frac{T_0}{\pi \alpha}} \tag{18}$$

where T_0 is the periodic cycle of temperature variation (h) ($T_0 = 24$ h) and e is the thickness of the sample (m).

The calculated time-lag as function of AF mass content is displayed in Figure 12 for samples with a thickness of 4 cm. As expected, one can notice that the time-lag increases with AF mass content increase. It reaches 2.21 h for an AF content of 5%. This means that the reinforcement of mortar with AF enhances the insulation performance of mortar.

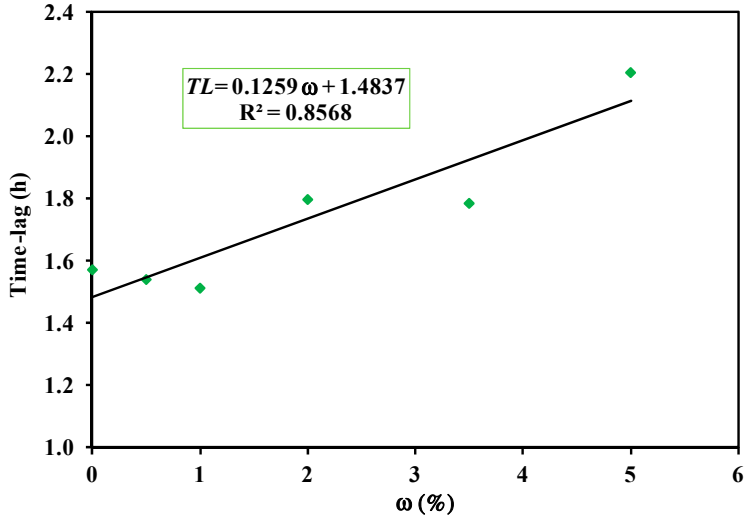


Figure 12. Time-lag variation as function of AF mass content.

Furthermore, Table 4 compares the time-lag of this AF-based composite with 5% to those of different materials used in the building construction sector. All compared materials have the same wall thickness of 20 cm. It can be seen that AFRM5% has a good time-lag. It is greater than that of hemp concrete (9.6 h) followed by cellular concrete (8.6 h). This result indicates that the composite AFRM material developed in this study can reduce outdoor weather conditions' propagation through the building envelope by about 10.37 h for a composite thickness of 20 cm. That is, the midday heat does not reach the indoor building until night and vice-versa for the mid-night cold.

Table 4. Comparison between the time-lag of AFRM 5% material and those of other materials presented in the literature.

Material (e = 20 cm)	ρ (kg·m^{-3})	R (W^{-1}·m^2·K)	α (m^2·s^{-1})	Time-Lag (h)
AFRM	1492	0.58	1.97×10^7	10.37
Hemp concrete	440	1.81	2.27×10^7	9.6
Cellular concrete	600	1.43	2.74×10^7	8.6
Earth block	1850	0.20	5.24×10^7	6.2
Solid brick	1950	0.23	5.41×10^7	6.3
Concrete	2300	0.11	7.93×10^7	5.1

3.4. Mechanical Performance Analysis

Figures 13 and 14 display the flexural and compressive strengths variation of composite with AF mass content.

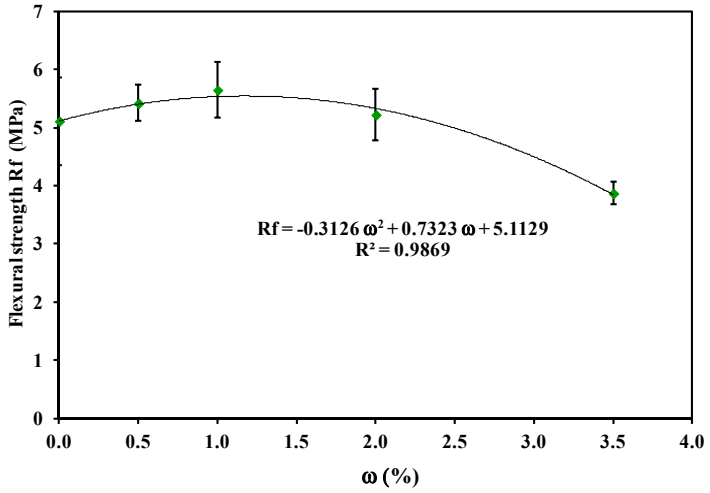


Figure 13. Flexural strength variation as function of AF mass content at day 28. Measurements uncertainty is below 8.5%.

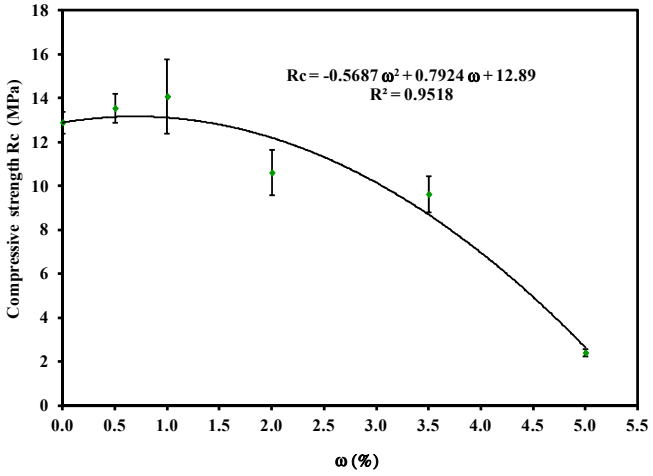


Figure 14. Variation of compressive strength with AF mass content at day 28. Measurements uncertainty is below 12%.

Concerning flexural strength (Figure 13), it is worth highlighting that it increases with the growth of the AF mass ratio from 0% to 1% where a maximum value of about 5.65 MPa is achieved. This improvement in flexural strength of about 10.45% is attributed to the good AF–mortar matrix adhesion as explained in Section 3.2, to the enhancement of mechanical bonds between solid matrix

(mortar) and reinforced AF, and to the high mechanical characteristics of AF, including high tensile strength and stiffness. However, for an AF ratio higher than 1%, it decreases to reach 3.87 MPa value for an AF mass ratio of 3.5%. This is due to the composite's porosity increase due to the excessive content of fibers in the mixture, resulting in a reduction of compactness and cohesion within the AF composite. This result is in agreement with previous research that dealt with mortar reinforcement with AF [48,49].

Compressive strength as a function of AF mass content is shown in Figure 14 with a measurement error of less than 12% for all specimens. It can be noticed that the compressive strength behavior is compatible with the flexural strength behavior as the AF mass content is increased. The maximum is obtained at a weight percentage of 1%. This maximum represents an increase of 9% in the compressive strength. Beyond this percentage, it decreases by around 82.5% at a weight fraction of 5%. This diminution is due to the growth in porosity which affects negatively the compressive strength.

3.5. Material Classification of the Developed Composite Based on Compressive Strength and Thermal Conductivity

The lightweight material classification can be made based on the compressive strength (Rc) and thermal conductivity (k). These two quantities are considered as crucial parameters in choosing suitable material types to be used in thermal insulation buildings. The diagram reported in Figure 15 represents a relationship between these two variables for each AF mass percentage. It can be noted that as AF mass content increases, the thermal conductivity of AFRM composite decreases considerably along with compressive strength, except AFRM1% for which Rc reaches a maximum value of about 14.07 MPa.

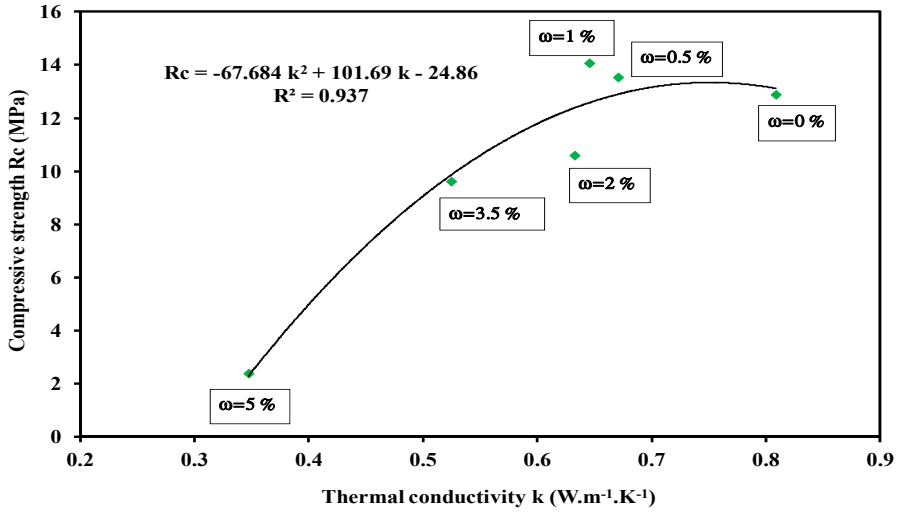


Figure 15. Correlation between compressive strength and thermal conductivity.

Thereafter, based on the functional classification of lightweight concrete of RILEM [50] (International Union of Laboratories and Experts in Construction Materials, Systems and Structures) and the results of Figure 15, this developed composite can be classified in two main classes as a function of AF mass content. Composites with Rc greater than 3.5 MPa and *k* less than 0.75 $W \cdot m^{-1} \cdot K^{-1}$ belong to Class II, while those with Rc greater than 0.5 MPa and k less than 0.3 $W \cdot m^{-1} \cdot K^{-1}$ are in Class III.

Using the transfer functions obtained from Figures 8 and 14, the composites built with a weight fiber percentage less than 4.8% can be classified among structural and thermal insulating materials of Class II while those built with higher fiber percentage can be good thermal insulating candidates and thus belong to Class III.

Finally, it has been shown from the results above that mortar reinforced with AF can be classified as a suitable candidate for exterior walls, partitions, ceiling, roofs and other building structural elements.

4. Conclusions

In this paper, mortar reinforced with alfa fiber for thermal insulating building construction was developed. The physical and thermal-mechanical properties of this new composite were investigated for AF mass ratio ranging from 0% to 5%. The analysis of the SEM pictures demonstrates that alfa fibers are randomly dispersed, separated, and well embedded in the mortar matrix which could indicate good bonds between AF and the surrounding solid matrix.

The addition of AF into mortar makes the new composite lighter by reducing its density by up to 15%, increasing its porosity by around 51% and improving its thermal conductivity by up to 57%. Comparison between the measured thermal conductivity and that predicted by Woodside–Messmer's model shows a good agreement, within 9.6%. This finding can help in the future to limit the need for thermal conductivity measurements if one has sufficient a priori information. Moreover, good heat damping properties were reached as the thermal diffusivity of the mortar-AF composite is decreased by up to 49% compared to the reference material. The incorporation of 0.5% to 1% of AF mass content leads to a better homogeneity and more consolidated structure within the composite. An enhancement of its mechanical properties by about 10.45% for the flexural strength and 9% for the compressive strength was observed. The composite samples with AF mass content less than 4.8% could be classified as structural and thermal insulating materials. Above 4.8%, it could be used as an insulating material.

In conclusion, this AF mortar composite, thanks to its simple manufacturing process, can be a very attractive material to be used in building in the Mediterranean region.

Author Contributions: Experiment planning, S.S.; experiment measurements and data analysis, S.S., L.B. and M.B.; theoretical models, L.B., M.B. and S.S.; writing-original draft preparation, S.S. and L.B.; writing-review and editing, L.B. and B.B. All authors have read and agreed to the published version of the manuscript.

Funding: This research received no external funding.

Conflicts of Interest: The authors declare no conflict of interest.

References

1. Pacheco, T.F.; Jalali, S. Cementitious building materials reinforced with vegetable fibres: A review. *Constr. Build. Mater.* **2011**, *25*, 575–581. [CrossRef]
2. De Carvalho Bello, C.B.; Boem, I.; Cecchi, A.; Gattesco, N.; Oliveira, D.V. Experimental tests for the characterization of sisal fiber reinforced cementitious matrix for strengthening masonry structures. *Constr. Build. Mater.* **2019**, *219*, 44–55. [CrossRef]
3. Ali, M.; Liu, A.; Sou, H.; Chouw, N. Mechanical and dynamic properties of coconut fibre reinforced concrete. *Constr. Build. Mater.* **2012**, *30*, 814–825. [CrossRef]
4. Seng, B.; Magniont, C.; Lorente, S. Characterization of a precast hemp concrete. Part I: Physical and thermal properties. *J. Build. Eng.* **2019**, *24*, 1–46. [CrossRef]
5. Elsaid, A.; Dawood, M.; Seracino, R.; Bobko, C. Mechanical properties of kenaf fiber reinforced concrete. *Constr. Build. Mater.* **2011**, *25*, 1991–2001. [CrossRef]
6. Nadhari, W.N.A.W.; Danish, M.; Nasir, M.S.R.M.; Geng, B.J. Mechanical properties and dimensional stability of particleboard fabricated from steam pre-treated banana trunk waste particles. *J. Build. Eng.* **2019**, *26*, 22–25. [CrossRef]
7. Belakroum, R.; Gherfi, A.; Bouchema, K.; Gharbi, A.; Kerboua, Y.; Kadja, M.; Maalouf, C.; Mai, T.H.; El Wakil, N.; Lachi, M. Hygric buffer and acoustic absorption of new building insulation materials based on date palm fibers. *J. Build. Eng.* **2017**, *12*, 132–139. [CrossRef]
8. Muhtar; Dewi, S.M.; Wisnumurti; Munawir, A. Enhancing bamboo reinforcement using a hose-clamp to increase bond-stress and slip resistance. *J. Build. Eng.* **2019**, *26*, 1–13. [CrossRef]
9. Kesikidou, F.; Stefanidou, M. Natural fiber-reinforced mortars. *J. Build. Eng.* **2019**, *25*, 1–6. [CrossRef]
10. Elhamdouni, Y.; Khabbazi, A.; Benayad, C.; Dadi, A.; Ahmid, O.I. Effect of fiber alfa on thermophysical characteristics of a material based on clay. *Energy Procedia* **2015**, *74*, 718–727. [CrossRef]

11. Rogge, E. Extraction et Etude des Propriétés Physiques et Mécaniques des Fibres d'Alfa (*Esparto grass*) en vue d'Applications Textiles. Master's Thesis, Ecole Nationale Supérieure d'Ingénieurs Sud-Alsace (UHA), Mulhouse, France, 2010.
12. L'alfa. Importance écologique et socio-économique. Portail de l'agriculture marocaine. *Terre Vie* **2002**, *61–62*, 1–3.
13. Couderc, R. Une «cueillette industrielle»: L'alfa en Algérie. *Méditerranée* **2016**, *19*, 3–16. [CrossRef]
14. Dallel, M. Evaluation du Potentiel Textile des Fibres d'Alfa (*Stipa Tenacissima* L.): Caractérisation Physico-Chimique de la Fibre au Fil. Ph.D. Thesis, Haute Alsace University, Mulhouse, France, 2012.
15. Korjenic, A.; Petránek, V.; Zach, J.; Hroudová, J. Development and performance evaluation of natural thermal-insulation materials composed of renewable resources. *J. Build. Eng.* **2011**, *43*, 2518–2523. [CrossRef]
16. Paiva, M.C. Alfa fibres: Mechanical, morphological and interfacial characterization. *Compos. Sci. Technol.* **2007**, *67*, 1132–1138. [CrossRef]
17. Mounir, J.; Slah, W.B.M.; Mohamed, B. Characterization of mechanical extracted alfa fibres. *Int. J. Fiber Text. Res.* **2014**, *4*, 1–4.
18. Krobba, B.; Bouhicha, M.; Zaidi, A.; Lakhdari, M. Formulation of a repair mortar based on dune sand and natural microfibers. *Concr. Solut.* **2014**, 91–95.
19. Jaballi, H.; Miraoui, S.; Hassis, I. Optimization of flexural strength and thermal conductivity of mortar reinforced with alfa fibers. *Appl. Mech. Mater.* **2015**, *799–800*, 794–799. [CrossRef]
20. El Hamdouni, Y.; Khabbazi, A.; Benayad, C.; Dadi, A.; Idriss Ahmid, O. Contribution to the thermal and mechanical behavior of the two materials at the base of clay reinforced by fibers ALFA and of straw fibers. *Res. J. Appl. Sci. Eng. Technol.* **2016**, *12*, 490–497. [CrossRef]
21. Braiek, A.; Karkri, M.; Adili, A.; Ibos, L.; Ben Nasrallah, S. Estimation of the thermophysical properties of date palm fibers/gypsum composite for use as insulating materials in building. *Energy Build.* **2017**, *140*, 268–279. [CrossRef]
22. Taoukil, D.; El Bouardi, A.; Ajzoul, T.; Ezbakhe, H. Effect of the incorporation of wood wool on thermo physical proprieties of sand mortars. *KSCE J. Civ. Eng.* **2012**, *16*, 1003–1010. [CrossRef]
23. Maghchiche, A.; Haouam, A.; Immirzi, B. Extraction and characterization of algerian alfa grass short fibers (stipa tenacissima). *Chem. Chem. Technol.* **2013**, *7*, 339–344. [CrossRef]
24. Kriker, A.; Debicki, G.; Bali, A.; Khenfer, M.M.; Chabannet, M. Mechanical properties of date palm fibres and concrete reinforced with date palm fibres in hot-dry climate. *Cem. Concr. Compos.* **2005**, *27*, 554–564. [CrossRef]
25. IMANOR. *Liants Hydraulique-Ciments Composition, Spécifications et Critères de Conformité*; NM 10.01.004; IMANOR: Rabat, Morocco, 2003.
26. AFNOR. *Essais Pour Déterminer les Caractéristiques Géométriques des Granulats—Partie 8: Évaluation des Fines—Équivalent de Sable*; NF EN 933-8 (NF P 18-622-8); AFNOR: Paris, France, 1999.
27. AFNOR. *Méthodes D'essai des Ciments, Partie I. Détermination des Résistances Mécaniques*; NF EN 196-1; AFNOR: Paris, France, 1995.
28. ASTM International. *Standard Test Methods for Apparent Porosity, Water Absorption, Apparent Specific Gravity, and Bulk Density of Burned Refractory Brick and Shapes by Boiling Water*; ASTM C20-00; ASTM Int.: West Conshohocken, PA, USA, 2000; Volume 3, PA 19428-2959.
29. Menguy, G.; Laurent, M.; Moutarda, A.; Leveau, J. *Cellule de Mesure des Caractéristiques Thermophysiques des Matériaux E1700. Société Weber Broutin*; Bulletin Technique, Deltalab: Carcassonne, France, 1986.
30. Boumhaout, M.; Boukhattem, L.; Hamdi, H.; Benhamou, B. Thermomechanical characterization of a bio-composite building material: Mortar reinforced with date palm fibers mesh. *Constr. Build. Mater.* **2017**, *135*, 241–250. [CrossRef]
31. AFNOR. *Techniques des Essais sur les Liants Hydrauliques*; NM 10.1.005; AFNOR: Paris, France, 1994.
32. Cabaleiro, D.; Nimo, J.; Pastoriza-Gallego, M.J.; Piñeiro, M.M.; Legido, J.L.; Lugo, L. Thermal conductivity of dry anatase and rutile nano-powders and ethylene and propylene glycol-based TiO_2 nanofluids. *J. Chem. Thermodyn.* **2015**, *83*, 67–76. [CrossRef]
33. Beck, J.M.; Beck, A.E. Computing thermal conductivities of rocks from chips and conventional specimens. *J. Geophys. Res.* **1965**, *70*, 5227–5239. [CrossRef]
34. Woodside, W.; Messmer, J.H. Thermal conductivity of porous media. I. Unconsolidated Sands. *J. Appl. Phys.* **1961**, *32*, 1688. [CrossRef]

35. Boutin, C. Conductivité thermique du béton cellulaire autoclavé: Modélisation par méthode autocohérente. *Mater. Struct.* **1996**, *29*, 609–615. [CrossRef]
36. Benazzouk, A.; Douzane, O.; Mezreb, K.; Laidoudi, B.; Quéneudec, M. Thermal conductivity of cement composites containing rubber waste particles: Experimental study and modelling. *Constr. Build. Mater.* **2008**, *22*, 573–579. [CrossRef]
37. Bederina, M.; Marmoret, L.; Mezreb, K.; Khenfer, M.M.; Bali, A.; Quéneudec, M. Effect of the addition of wood shavings on thermal conductivity of sand concretes: Experimental study and modelling. *Constr. Build. Mater.* **2007**, *21*, 662–668. [CrossRef]
38. Mark, C.; Burns, P.J.; Sommerfeld, R.A. Quasi-steady temperature gradient metamorphism in idealized, dry snow. *Numer. Heat Transf. Part. A Appl.* **1994**, *25*, 259–278.
39. Maxwell, D.C. *A Treatise of Electricity and Magnetism*, 3rd ed.; Dover Publications Inc.: New York, NY, USA, 1954; Volume 1–2.
40. Krischer, O. *Die Wissenschaftlichen Grundlagen der Trocknungstechnik*; Springer: Berlin/Heidlberg, Germany, 1963; Volume 1.
41. Dawood, E.T.; Ramli, M. Properties of high-strength flowable mortar reinforced with palm fibers. *Int. Sch. Res. Netw.* **2012**, 1–5. [CrossRef]
42. Belhadj, B.; Bederina, M.; Makhloufi, Z.; Goullieux, A.; Quéneudec, M. Study of the thermal performances of an exterior wall of barley straw sand concrete in an arid environment. *Energy Build.* **2015**, *87*, 166–175. [CrossRef]
43. Taallah, B.; Guettala, A. The mechanical and physical properties of compressed earth block stabilized with lime and filled with untreated and alkali-treated date palm fibers. *Constr. Build. Mater.* **2016**, *104*, 52–62. [CrossRef]
44. Bal, H.; Jannot, Y.; Gaye, S.; Demeurie, F. Measurement and modelisation of the thermal conductivity of a wet composite porous medium: Laterite based bricks with millet waste additive. *Constr. Build. Mater.* **2013**, *41*, 586–593. [CrossRef]
45. Rahim, M.; Douzane, O.; Tran Le, A.D.; Langlet, T. Effect of moisture and temperature on thermal properties of three bio-based materials. *Constr. Build. Mater.* **2016**, *111*, 119–127. [CrossRef]
46. Boukhattem, L.; Boumhaout, M.; Hamdi, H.; Benhamou, B. Moisture content influence on the thermal conductivity of insulating building materials made from date palm fibers mesh. *Constr. Build. Mater.* **2017**, *148*, 811–823. [CrossRef]
47. Chikhi, M. Young's modulus and thermophysical performances of bio-sourced materials based on date palm fibers. *Energy Build.* **2016**, *129*, 589–597. [CrossRef]
48. Krobba, B.; Bouhicha, M.; Kenai, S.; Courard, L. Formulation of low cost eco-repair mortar based on dune sand and Stipa tenacissima microfibers plant. *Constr. Build. Mater.* **2018**, *171*, 950–959. [CrossRef]
49. Miraoui, I.; Jaballi, S.; Hassis, H. Analysis of the mechanical properties of mortar reinforced with long unidirectional alfa fibers in different curing conditions. *Mech. Compos. Mater.* **2016**, *52*, 545–554. [CrossRef]
50. Rilem, L. Functional classification of lightweight concrete. *Mater. Struct.* **1978**, *11*, 281–283.

Publisher's Note: MDPI stays neutral with regard to jurisdictional claims in published maps and institutional affiliations.



© 2020 by the authors. Licensee MDPI, Basel, Switzerland. This article is an open access article distributed under the terms and conditions of the Creative Commons Attribution (CC BY) license (http://creativecommons.org/licenses/by/4.0/).